Journal of Material and Process Technologies

Available online at http://journal.aastu.edu.et/

Synthesis And Characterization of Modified Silica Gel Supported Silver Nanoparticles using Batch Studies for Disinfection of Escherichia Coli and Staphylococcus Aureus for Drinking Water

Belete Tessema[a,], Girma Gonfa[a,b] Sintayehu Mekuria Hailegiorgis[a], Meroda Tesfaye Gari[a]*

[a]Department of Food Science and Applied Nutrition, Addis Ababa Science and Technology University, 16417 Addis Ababa, Ethiopia

Biotechnology and Bioprocessing Center of Excellence, Addis Ababa Science and Technology University, Addis Ababa, Ethiopia. Box 16417

Article Information

Article history:

Received 7 November 2024

Received in revised form 23 December 2024

Accepted 24 December 2024

Keywords:

Teff straw ash

Modified silica gel

Silver nanoparticles

Drinking water

Disinfection

**Corresponding author.*

E-mail: beletetessema@gmail.com (B. Tessema)

https://doi.org/10.69660/jmpt.v1i2.86

Abstract

AgNPs were synthesised using Vernonia amygdalina leaf extract as a reducing agent in an $AgNO_3$ solution. The synthesized AgNPs solution was characterized and used for the synthesis of modified silica gel (MSG)-supported AgNPs (MSG-AgNPs). After being treated with HCl, the grounded Filagot teff straw was calcined for 2 h at 500, 600, 700, 800, and 900 °C. The sol-gel method was used to create the silica gel, and NaOH solution was used to treat it. An 80.4% SG yield with a 99.39% purity and the largest surface area (807.163 m^2/g) were obtained at 700 °C and were chosen for additional analysis. Trimethylchlorosilane (TMCS)/ethanol/hexane was then added to SG at volume/vol ratios of 15/25/100, 25/25/100, 35/25/100, and 50/25/100. A modified SG mixture of TMCS/ethanol/hexane with a maximum surface area of 510.4 m^2/g was produced at 25/25/100 (vol/vol) of the mixture. Using the sol-gel process, the AgNPs that were produced with Vernonia amygdalina leaf extract were impregnated on the MSG. Prior to impregnating AgNPs onto the MSG, several quantities of AgNPs (1.5, 3, 6, and 9 mM) were made. The solutions were then supplemented by MSG. For 1.5, 3, 6, and 9 mM solutions, the MSG-AgNPs composites had surface areas of 475.0, 457.3, 438.5, and 410.9 m^2/g, respectively. Finally, batch disinfection experiments against S. aureus and E. coli were conducted. In the batch research, MSG-AgNPs impregnated with 9 mM AgNPs reduced the concentration of E. coli from 10^4 and 10^5 to 0.0 CFU/mL in 10 min and from 10^6, 10^7, and 10^8 to 0.0 CFU/mL in 60 min.

1. Introduction

Waterborne pathogens pose a significant public health risk as they are bacteria that can cause diseases when they contaminate groundwater and surface water sources. These pathogens can enter water systems through various means, including human or animal waste, agricultural runoff, sewage leaks, or after natural disasters. Common waterborne bacteria include Escherichia coli, S. aureus, Shigella spp., Salmonella spp., Vibrio spp., and Cryptosporidium. Drinking water contaminated with these bacteria can lead to infections affecting the gastrointestinal tract, skin, bloodstream, and other organs [1-4]. Based on the study results of El-Aassar et al. [5] and Phong et al. [6], several chemicals are frequently used in the treatment of drinking water in order to reduce bacterial contamination. Substances including ozone, free chlorine, iodine, and chloramines are frequently used. Their propensity to react with organic matter found in nature or other substances found in water, resulting in the creation of disinfection byproducts (DBPs), is a significant cause for worry [7, 8]. Metal nanoparticles such as silver, zinc, copper, gold, cerium dioxide, and titanium dioxide have several uses in the field of water treatment because of their unique physical and chemical properties. These tiny particles have the ability to break down organic pollutants, remove heavy metals, sanitize microorganisms, and support bioremediation initiatives [9-12]. It was also observed that AgNPs have indicated strong antibacterial activity and preferred for drinking water treatment. However, AgNPs some limitations when applied to drinking water treatment without further modification. Such limitation is reported to be it clumped together during application, it easily loses stability or leaches out into the water body during its use, and it easily releases silver ions into the water [13-15]. AgNPs have encouraging uses in water filtration, but a number of barriers prevent their widespread use. The propensity of AgNPs to aggregate limits their effectiveness, while worries about their stability, toxicity, and environmental imprint present substantial challenges [14, 16, 17]. It is beneficial to combine silver nanoparticles (AgNPs) with a range of materials in order to increase the effectiveness of water disinfection [18, 19]. To reduce such limitations of AgNPs, it can be integrated with polymers, granular activated carbon, ceramic filters, filter membranes, and silica. It was also reported that silica-based materials are particularly suitable for stabilizing nanoparticles for biological applications, as they have several advantages such as biocompatibility, high chemical and thermal stability, and hydrophilic nature. In the present research work, modified silica gel-supported silver nanoparticles (MSG-AgNPs) were

synthesized as a disinfectant for the treatment of drinking water. Problems like poor dispersity and biocompatibility can make them impractical, which means further study is needed to solve these obstacles and realize their full potential [20-24]. Because silica-based materials have great chemical and thermal stability, are hydrophilic, and are biocompatible, they are especially well suited for stabilizing nanoparticles for biological applications [20, 25, 26].

The industrial synthesis of silica necessitates elevated thermal conditions, often reaching up to 1700 °C, which underscores the challenges of commercial scalability. Utilizing high-purity silica for industrial purposes incurs considerable expense. Furthermore, the production process poses significant health risks. Prolonged inhalation of crystalline silica dust can precipitate silicosis, a condition that has been linked to severe respiratory ailments such as lung cancer, emphysema, and pulmonary tuberculosis [27-29]. This has led to a great deal of attention in the search for alternative reduction origins and precursors. Because of this restriction, precursors rich in silica gel, including rice husk, bamboo leaf, rice straw, sugarcane bagasse, wheat straw, maize leaves, and teff straw [29-31] were used.

There are many advantages of synthesizing silica gel from biomass resources, two of which are lower manufacturing costs and more environmental sustainability [32-34]. In this study, teff straw was treated with HCl, then washed until the pH reached 7, dried in an oven, and thermally treated. The ash from the teff straw was then used to synthesize silica gel using a NaOH solution. In a different study, bio-based silica gel was prepared using the sol-gel method from a variety of sergegna (white and brown mixed) TS with unknown species, yielding 91 to 92% [33, 35, 36].

Drinking water is a vital resource for all living things as well as non-living ones, yet microbiological pollution poses serious problems. This study suggests a novel strategy that combines the incorporation of modified silica gel (MSG) with the production of silver nanoparticles (AgNPs) from Vernonia amygdalina leaf extracts. The synthesis of AgNPs is made more affordable and environmentally friendly by using plant extracts as reducing and stabilizing agents. The addition of MSG, which is accomplished using the sol-gel process, increases AgNPs' stability and dispersibility while also enhancing their antibacterial activity against a variety of infections. Until now, the antibacterial efficacy of MSG enhanced with AgNPs in batch disinfection studies tests against bacteria has not been investigated. This work aims to fill in this knowledge gap.

2. Materials and methods

2.1. Chemicals and Materials

Filagot (red), Dagim, Kuncho and Kora (white) teff straws were obtained from the Debre Zeit Research Centre, Ethiopia. The teff straw was transported to the Ababa Science and Technology University laboratory in a polyethylene bag. Hydrochloric acid (HCl, 37%) was obtained from Loba Chemie Pvt. Ltd. (India). Sodium hydroxide (NaOH, 96%) was obtained from Abron Chemicals Ltd. (India). Anhydrous ethanol (EtOH, 99.9%) was obtained from Favor Trading plc (Taiwan). Aqueous ammonia (NH3.H2O, 30%) was obtained from Neolab Pvt. Ltd. Trimethylchlorosilane (C_3H_9ClSi, 98%, Cisco Research Laboratory Pvt. Ltd., USA) was obtained from Cisco Research Laboratory Pvt. Ltd., USA. N-hexane (C6H14, 99%) was obtained from Atico (India). The chemical analyses were performed to determine the composition of the teff straw. The compositions of the TS and TSA were carried out using atomic absorption spectroscopy (CB-AAS-3510).

2.2. Methods

2.2.1. Teff straw sample preparation

The teff straw (TS) underwent a cleaning process to remove any impurities, such as leaves, sand, dirt, and clay. After soaking in tap water for 24 h, the straw was washed five times with tap water to eliminate any remaining dirt and muck. The straw was then dried under the sun. The dried straw was ground using a high-speed grinder to obtain a fine powder with a particle size of less than or equal to 2 µm. The powder was kept in sealed polyethene bags until further use.

2.2.2. Characterization of teff straw

2.2.2.1. Proximate analysis experiment

Proximate analysis is a vital process in evaluating the quality and usability of fuel sources, particularly biomass and coal. By determining the moisture, volatile matter, ash, and fixed carbon content, researchers can infer the combustion characteristics and efficiency of the material. The ASTM D 3173 standard for moisture determination is a widely recognized method, ensuring that the results are accurate and reliable for further analysis and application in various industries [37], the volatile matter using ASTM D-3175 [38], the ash content using ASTM D-3174 [39].

2.2.2.2. Thermogravimetric and FTIR analyses of teff straw

The thermogravimetric analysis (TGA) of a teff straw sample was conducted using an SDT Q600 thermographic analyzer. The sample, weighing 10 mg, was placed in a platinum crucible and subjected to a controlled heating rate of 20 °C/min, from room temperature up to 900 °C. Subsequently, Fourier-transform infrared spectroscopy (FTIR) analysis was performed using a Thermo Scientific ATR-FTIR, IS50 instrument, scanning across a wavelength range of 4000-650 cm^{-1} to identify the different chemical bonds present in the sample.

2.2.3. Preparation of teff straw ash

Teff straw ash was produced using the method reported by Bageru and Srivastava [33] and Kalapathy et al. [40], with some modifications. The process described involves the acid treatment of teff straw, a byproduct of the ancient grain, teff, commonly used in Ethiopian cuisine. The treatment with hydrochloric acid (HCl) aims to purify the material by removing various metal impurities and their oxides. This step is crucial for preparing the straw for further applications, possibly in the production of biofuels or bioplastics, where purity is essential for the efficiency and quality of the final product [35, 41]. Then, the sample was washed with distilled water several times to neutralize the HCl acid from the straw. Washing was performed until pH reach 7.0. The sample was then dried in an oven at 100 + 5 °C. The acid-treated teff straw was calcinated in programmable muffle furnace. Calcinations were performed over various calcination temperature (500, 600, 700, 800 and 900 °C) and calcination times (2, 3, 4, and 5 h). Finally, teff straw ash has been cooled inside desiccators to room temperature and kept in airtight container until further use. The surface area of teff straw ash was determined using Brunauer-Emmett-Teller (SA-9600 series, HORIBA, USA). X-ray diffractometer (RIGAKU-Model: Ultima-IV, USA) was used to see crystallinity the ash.

2.2.4. Silica gel preparation and characterization

2.2.4.1. Silica gel preparation

Silica gel was produced using the method reported by Bageru and Srivastava [33] and Kalapathy et al [40], with some modifications. Teff straw ash (10g) each was transferred 250 mL Erlenmeyer flasks and then 80 mL 2.5 N NaOH was added to the flaks. The flask was covered with aluminum foil and heat at 90 + 5 °C for 1 h under constant magnetic stirring. Then, the solution was cooled at room temperature and then filtered through Whatman No. 41 ash-less filter paper. Then, it was washed with 100 mL boiling water. The NaOH treatment helps to leach out silica from the ash as sodium silicate as depicted in equation (1) [42].

$$SiO_2(ash) + 2NaOH \rightarrow Na_2SiO_3 + H_2O \quad (1)$$

The filtrate was heated on a hot plate at a temperature of 90 + 5 °C for 1 h and then been cooled to room temperature. The cooled filtrates were titrated with as solution of 2.5 N HCl with magnetic stirrer until pH reduced from 13.3 to 7. When pH became below to 10, the silica gel started to precipitate and the mechanism is depicted in equation (3.6) [42].

$$Na_2SiO_3 + 2HCl \rightarrow SiO_2 + 2NaCl + H_2O \quad (2)$$

The solution was aged in the mother solution at room temperature for 20 h to obtain silica gel. To remove the salt (NaCl), the precipitate silica gel was repeatedly rinsed in distilled water. Then, distilled water added, heated to 35 ^{0}C with mechanical stirring to break down formed slurry. Next, the slurries were then centrifuged for 15 min at 2500 rpm, the clear supernatant was discarded and the washing step was repeated. Finally, the silica gel was placed in a beaker and dried at 90 °C for 12 h. The dried silica gel was grounded into powder using a pestle and mortar and stored in airtight polyethylene bag for further use.

2.2.4.2. Characterization

The surface area, pore volume and pore size of silica gel samples was measured using Brunauer-Emmett-Teller (Nova 4000e, Quantachrome, USA)). FTIR spectroscopy (Thermo Scientific FTIR, IS50) was used to record the spectrum data within the range of 4000-400 cm^{-1}. X-ray diffractometer (RIGAKU-Model: Ultima-IV, USA) was used to see crystallinity the silica gel. The XRD pattern was collected using Cu Kα radiation at a current of 44 mA at 2θ over 3 to 80°, an acceleration voltage of 40 kV, and a speed of 10.0 degrees per minute. A scanning electron microscopy (JEOL Model JSM 63-90, USA) equipped with EDX was used to analyses the surface morphology of silica gel.

2.2.5. Modified silica gel preparation and characterization

2.2.5.1. Modified silica gel preparation

Acid (HCl) was gradually added to an aqueous sodium silicate solution of initial pH of 13.5 which was prepared using the method presented in section 3.3.4 above until its pH reduced to 4 to 4.5. To avoid the formation of a gel-like substance, this procedure was performed rapidly with continuous agitation. The solution was then put into a container with a 1 M aqueous ammonia solution. The pH of the solution increased to pH of 5–6 to form a gel. To improve the gel network, the gels were aged for 24 h at 50 °C using the method reported by Abdul Halim et al. [43], [44]. Sodium ions were removed from the gel by passing water vapor through the hydrogels using the method reported by [45]. To remove the water from the pores, the prepared silica wet gels were submerged in ethanol and shaken in a water bath for 12 h at 50 ^{0}C [46]. Next, the ethanol was extruded with hexane for additional 12 h.

For surface modification, the silica wet gel was submerged and kept in sonicator in a water bath for 12 h at 50^{0}C in a solution of TMCS, ethanol, and hexane. TMCS, ethanol, and hexane of various volumetric ratios of 0.15:0.25:1, 0.25:0.25:1, 0.35:0.25:1, and 0.50:0.25:1 for TMCS/ethanol/hexane ratio. The TMCS treated silica gel was first dried for 2 h at 80 °C in an oven to remove any lingering TMCS and the other solvents. It was then added 500 mL of distilled water and sonicated for 10 min. Next, it was dried for 18 h 85 + 5, then for 6 h at 145 + 5 ^{0}C and finally for 24 h for 50 + 5 ^{0}C as suggested by other authors [3]. Finally, the prepared modified silica gel grounded using mortar and for further analysis and uses.

2.2.5.2. Characterization of modified silica gel

The surface area of the modified silica gel was determined using Brunauer-Emmett-Teller (SA-9600 series, HORIBA, USA). FTIR spectroscopy (Thermo Scientific FTIR, IS50) was used to record the spectrum data within the range of 4000-400 cm^{-1}. X-ray diffractometer (RIGAKU-Model: Ultima-IV, USA) was used to study crystallization or amorphous phase analysis. The XRD patterns were collected using Cu Kα radiation at a current of 44 mA at 2θ over 3 to 80°, an acceleration voltage of 40 kV, and a speed of 10.0 degrees per minute. A scanning electron microscopy (Inspect F50 SEM, Japan) equipped with EDX was used to analyses the surface morphology of modified silica gel.

2.2.6. Synthesis of silver nanoparticles

The silver nanoparticles (AgNPs) were prepared using Vernonia amygdalina leave extract. First, the leaves were washed with distilled water and shade-dried for a week. Next, the dried leaves were grounded using a coffee grinder. Then, a 250 mL conical flask was filled with 200 mL of distilled water and 20 g of the leaf powder was added, and boiled for 20 minutes at 90 + 5 °C. Finally, the solution was vacuum-filtered through Whatman filter paper (No. 1, 90 mm, UK), and stored in a refrigerator at 4 °C utile it is used for synthesis of the AgNPs. `

For synthesis of AgNPs, vernonia amygdalina leave extract (10 mL) added to four different flasks, each containing 100 mL of distilled water and different $AgNO_3$ concentration (1.5, 3, 6, and 9 mM). The flasks placed on hot plate and the temperature of water in the vessel was kept at 65 + 5 °C for 15 minutes under continuous magnetic stirring. The formation of AgNPs was indicated by color of the solution, that is, from colorless to light grey. After the color change was observed, the flasks were removed from the heating plates. To prevent AgNPs from clumping together, the flasks kept under stirring magnetic stirrer the solutions cooled to room temperature. Then, the samples were refrigerated at 4 °C for 24 h and exposed to ultrasound waves (Sonorex Digiplus DL-Ultrasonic Baths, Bandelin, Germany) for 15 min. The solutions were cooled and stirred until they became a light grey colloidal solution, indicating that the AgNPs reduction process was successful [47].

2.2.7. Characterizations of modified silica gel supported silver nanoparticle

The modified silica gel-supported AgNPs were examined using UV-Vis spectroscopy (Jasco V-770, UV-Vis-JASCO Co., Tokyo, Japan) range of 200 to 600 nm. FTIR spectroscopy (Thermo Scientific FTIR, IS50) was used to record the spectrum data within the range of 4000-400 cm^{-1}. X-ray diffractometer (RIGAKU-Model: Ultima-IV, USA) was used to see the

crystallinity. The XRD patterns were collected using Cu Kα radiation at a current of 44 mA at 2θ over 3 to 80^0, an acceleration voltage of 40 kV, and a speed of 10.0^0/min. Scanning electron microscopy (JEOL-Model: JSM-6390, USA) equipped with EDX was study the surface morphology of modified silica gel-supported AgNPs. The surface area of modified silica gel supported AgNPs was measured using Brunauer-Emmett-Teller (SA-9600 series, HORIBA, USA).

2.2.8. Antibacterial Performance Evaluation

2.2.8.1. Inoculum preparation

Brain-heart infusion broth (38 g) was inserted into 1000 mL of sterilized distillate water and autoclaved. Then, after being infused into fresh medium, E. coli and S. aureus cultures were cultured at 37 °C for 24 h to get the strains to the exponential growth phase. The cells were then taken from the effluent, centrifuged at 10,000 rpm for 5 min, rinsed with sterilized distillate water, and then centrifuged once more and re-suspended in sterilized water. In addition, a 0.5 McFarland turbidity standard was made from a solution containing a combination of 1% H_2SO_4 and 1% barium chloride dihydrate. The cultures were removed from colonies by touching them with a loop and transferring them to saline, or by removing them from broth suspension and transferring them to saline, and then adjusting them to be the same as a 0.5 McFarland standard. This was done in well-lit conditions by comparing how black lines appeared through the inoculum. The most frequently isolated organisms are estimated to have 1.5 x 108 CFU/mL in a properly adjusted solution. In a similar manner, 1000 mL of sterilized distillate water was mixed with 38 g of Mueller-Hinton agar, then placed in a biosafety cabinmate. Then, for each bacterial growth on the media for 24 h, 100 µm of E. coli and S. aureus were taken. For the prepared modified silica gel-supported AgNPs of A, B, C, and D, 2.5, 5, 10, 20, 30, 40, and 50 mg/mL of each prepared sample were added. The modified silica gel-supported AgNPs were resuspended in solvent-sterilized distilled water, sonicated, and autoclaved to create the solution of the modified silica gel-supported AgNPs [48, 49]. All the experiments were conducted in triplicate.

2.2.8.2. Batch antibacterial activity test

Nutrient agar (32 g) nutrient agar was poured into 1000 mL distillate water and sterilized. Then, the modified silica gel supported AgNPs (MSG-AgNPs) designated as A, B, C, and D added to distilled water forming concentration of 40 mg/mL (MSG-AgNPs/water). The samples were then inserted in a shaking incubator with 150 rpm at 37 °C under mixing. Then, the samples were inserted in an autoclave for 15 min of sterilization at 121 °C. Next, 20 mL of MSG-AgNPs were poured into the sterilized petri dishes and allowed to cool to room temperature for 24 h in the sterile environment. The cultured E. coli and S. aureus cells were dispersed in PBS (phosphate buffer saline), with a cell concentration of 108 CFU/mL in the exponential growth phase adjusted by the 0.5 MacFarland standard, as explained previously in the inoculum preparation. The cells were further diluted to an initial concentration of 107, 106, 105, and 104 CFU/mL. MSG-AgNPs (40 mg) was added to 1.0 mL of this cell suspension of samples A, B, C, and D. This was incubated and maintained at 150 rpm at 37 °C using a rotating shaker to prevent any settling of granules. Then, 100 µL E. coli and S. aureus were taken for each bacterium culture on the prepared media. All the experiments were conducted in triplicate.

The effect of initial concentrations of E. coli and S. aureus bacteria concentration, effect of MSG-AgNPs dosage and effect of inactivation (disinfection) time were studied. The effect of initial bacteria concentrations was investigated over 104 to 108 CFU/mL, the effect of MSG-AgNPs dosage was studied over 30 to 50 mg/mL and the disinfection time was assessed over 10, 20, 30, and 60 min [5]. Inactivation of E. coli and S. aureus were determined by calculating viable cell count CFU/mL using the spread plate technique and the percentage of reduction (death rate) was calculated using in equation (10) [16].

$$\text{Reduction } \% = \frac{(N_O - N_t)}{N_o} * 100 \qquad (3.5)$$

where, N_t is the number of CFU/mL at any defined time, and N_0 is the initial number of CFU/mL.

3. Results and discussion

3.1. Proximate Analysis

The proximate analysis has been reported in the range of 7.40% to 9.20% indicates a relatively consistent moisture level across the different varieties, which is beneficial for standardizing processing and usage [50]. This consistency also reflects well on the methods used for harvesting and storing the teff straw, suggesting that they are effective in maintaining an optimal moisture content that aligns with previously reported values [33, 51, 52]. The moisture content of teff straw, which ranges from 6.00 to 9.38, is indeed comparable to other dried biomasses. This moderate moisture level makes teff straw a versatile material for various uses, including as a renewable energy source. The variability in moisture content, influenced by the teff variety, highlights the importance of selecting the appropriate type for specific applications, ensuring efficiency and sustainability in its use [53]. The moisture content in biomass is indeed a critical factor that influences its quality as a source of energy. It's interesting to note the variation in volatile matter content among different teff straw varieties, with Kora teff showing the highest and Kuncho the lowest percentages. These differences can be attributed to the inherent properties of each variety as well as the drying techniques employed. Continuous research and comparison with past data are essential for optimizing biomass for energy production. The slight increase in volatile matter in current teff straw varieties could suggest a change in either the biomass characteristics [33].

The ash content, which slightly varies between 6.00% to 6.34% among different varieties, is a critical factor in determining the quality and yield of biosilica. Studies have shown that the purity of biosilica extracted from teff straw ash can exceed 99% when prepared at higher ashing temperatures. This highlights the agricultural and industrial significance of teff straw, not only as livestock fodder but also as a valuable resource for sustainable material production [33], 4.6 [51], 5 [54] and 5.88 [55]. The observation that the current teff straw varieties have a higher ash content than those previously studied could have significant implications for both agricultural practices [33, 51, 54-56].

It's interesting to note that the studied teff varieties have similar ash contents, which indicates a level of uniformity in their composition. This uniformity can be beneficial for large-scale agricultural practices. The general variation of ash content in biomasses from 2% to 22% [53]. Teff straw, a byproduct of the ancient grain predominantly grown in Ethiopia, presents a medium ash content relative to other biomasses. This

characteristic suggests its suitability for extracting valuable inorganic components like silica and various metal oxides, which are essential in numerous industrial processes. Moreover, the fixed carbon content of teff straw, ranging from 13.40% to 16.67% across different varieties, aligns with previously reported data, affirming its consistency and potential as a biomass resource [33]. The fixed carbon content of teff straw, an important parameter in assessing its quality as a biomass, shows interesting variations. This range of 8% to 31% for biomasses indicates a significant diversity, which can influence their suitability for different uses, such as biofuel production or soil amendment. Understanding these variations is crucial for optimizing the use of teff straw in various agricultural and energy sectors [53]. Teff straws' high volatile matter content may be the cause of their lower fixed carbon content since biomass with a high volatile matter content is expected to have a lower fixed carbon content.

Table 1: Moisture, volatile, ash and fixed carbon contents of dried teff straws.

Biomasses	Moisture	Volatile	Ash	Fixed carbon
Dagim	9.20	78.00	6.34	14.86
Kuncho	9.00	77.00	6.34	16.67
Kora	7.80	80.20	6.34	13.47
Filagot	7.40	80.60	6.00	13.40

3.2. Chemical Composition

The composition of the biomass lost in ash deposits is represented by the loss upon igniting. The Filagot, Kora, Dagim, and Kuncho kinds of teff straw have silica concentrations of 5.92, 5.66, 4.94, and 4.70%, in that order [41, 50]. This translates to silica concentrations in the ashes made from the Filagot, Kora, Dagim, and Kuncho types of 92.21, 91.59, 77.19, and 87.20%, respectively. This demonstrates how the types of teff affect the amount of silicon in teff straw. Furthermore, teff straws have a high silicon concentration that is similar to other biomasses with high silica content, such wheat and rice husk. There were recorded silica values of 92.81% and 92.30% for rice and wheat husk, respectively [53, 57]. The ashes from teff straw also contain metal oxides, such as MgO and CaO, which are typically categorized as macronutrients, in addition to silica. For the teff straws under study, the percentages of metal and alkali species in the ashes are 7.79, 8.41, 12.80, and 22.81% for Filagot, Kora, Kuncho, and Dagim, in that order. Crop residue ashes typically have an alkali oxide concentration ranging from 5% to 64% [50, 53]. High silicon crop residue ashes typically contain a high proportion of alkali oxides. Elevated concentrations of metal and alkali metals impact not just the silica concentration but also the silica extraction process from the ashes. Methods like hydrolysis based on acids or alkalis or chelation reactions based on carboxylic groups can be employed to extract the metal and alkali from the ash and refine the silica [58-60].

3.3. Thermogravimetric analysis

Figure 1 (a) displays the results of the thermogravimetric examination of the teff straw collected from the four teff types. Three primary areas of weight loss are visible on the thermogravimetric analysis curve. Dehydration, or the elimination of moisture, occurs in the zone before 200 °C, while volatilization, or the release of volatile substances, occurs in the range that follows up to 400 °C. The evolution of light volatiles may occur concurrently with the dehydration stage [61]. The carbonization (combustion of flammable materials) that occurs in the region above 500 °C. The teff straws' weight loss trend is comparable to thermogravimetric assessments of the majority of biomasses [50, 62, 63].

The initial phase saw weight losses of 6.25% for the Kora variety, 5.00% for Kuncho, and 4.50% for the Filagot and Dagim kinds. In the second (volatilization) stage of the thermal decomposition, there were significant mass losses. For Kora, Kuncho, Filagot, and Dagim, the weight reduction in the second stage is 62.25%, 61.50%, 57.10%, and 56.00%, respectively. While the weight loss at a given temperature differs across the four kinds, the thermographic curve of the teff straw displays comparable tendencies.

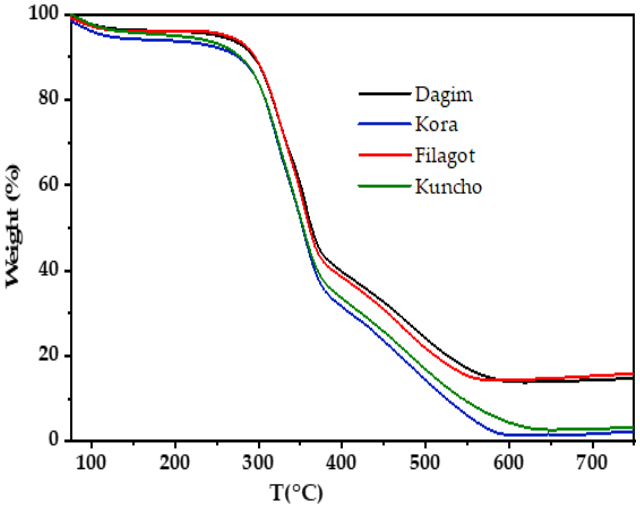

(a)

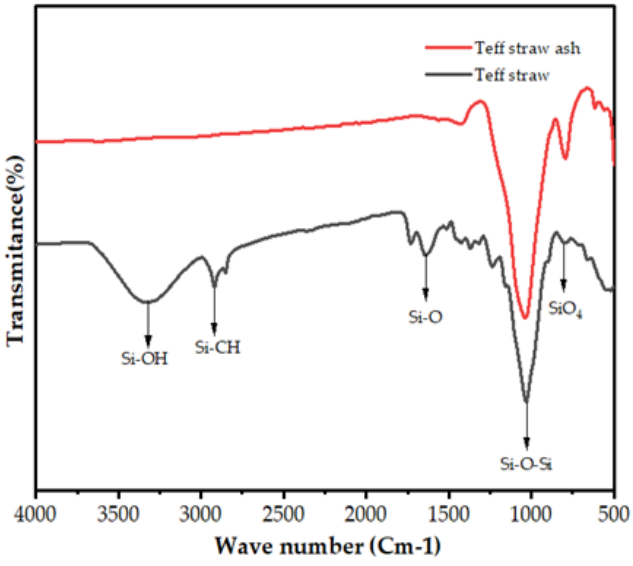

(b)

Fig. 1. (a) TGA of TS and (b) FTIR spectra of Filagot TS and TSA of teff straw varieties.

3.4. Fourier Transforms Infrared Spectroscopy

FTIR was used to analyzed the functional groups of the raw teff straw and the ashes that resulted. Teff straw and the ashes had various functional

groups with wavenumbers ranging from 400 to 4000 cm^{-1}. Figure 1 (b) depicts the FTIR spectra of the straw and the ash that resulted for the Filagot variety. The teff straw's OH stretching band is represented by the peak at a wavenumber of 3380 cm^{-1}. The C-H stretching is indicated by the band at 2923 cm^{-1} [64]. The carboxylic and carbonyl groups from aldehydes, ketones, and aromatic rings mostly from the lignin component were identified as the source of the peak detected at 1730 cm^{-1} [54]. The cause was O-H bond bending vibration because of the broadband at wave numbers ranging from 1633 to 1645 cm^{-1}. An intense and discernible absorption peak had accumulated in the band on wave number from 1036 to 1044 cm^{-1}, which was caused by the asymmetric stretching of the Si-O-Si (siloxane) bonding [65]. The broad band between 3000 and 3700 cm^{-1} was assigned to the asymmetric stretching and bending vibrations of silanol - OH groups (Si-O-H), whereas the broad band at 1637 cm^{-1} belonged to H-O-H bending [51]. Figure 1 (a) shows the FTIR spectrum of the ash from the Filagot variety of straw. The strong peaks at 1100 cm-1 demonstrate the shear bands and asymmetric stretching vibration of the Si-O-Si bonds [66]. Si is responsible for the band at 800 cm^{-1} because of SiO_4's symmetric stretching vibrations [64]. The peaks for the teff straw in Figure 3's range of 3750–2500 cm^{-1} vanished into the resultant ashes. This is because heat treatments eliminated the organic components that included hydroxyl functional groups and the water present in the biomass. The FTIR spectra exported by earlier writers and the resultant ashes from the contemporary teff straw are comparable [52, 64].

3.5. Silica gel yield

The findings demonstrate that amorphous silica gel has been generated from TSA using a sol-gel method with yields of 57.2, 79.7, 80.4, 94.2, and 87.3% for calcination temperatures varying from 500, 600, 700, 800, and 900 °C respectively, with calcination time of 2 h. From the results, it is well apparent that the TS can be a sustainable and promising and bio-precursor for silica-gel. The silica gel yield ranges from 57.2 to 94.2%, as shown in Figure 6. The current precursors collected from Debre Zeit Research Center have shown larger silica gel production compared with the previous studies reported from TS collected from local farmers the results varying from 49.5-84.5% [33] and 59.38-85.85% [52]. The highest silica gel yield of the current precursor was greater than the silica gel yield reported for other feedstock, such as palm shell (92.00 wt %) [67]. The greatest yield from the TS was, however, marginally lower than that of rice husk which has been recorded to be greater than 95.00% [68]

3.6. Characterization of silica gel

3.6.1. Surface area, pore volume and pore size analysis using BET

The temperature at which teff straw ash is calcined has an impact on its specific surface area. The particular surface area steadily drops as the temperature rises. Compared to other feedstocks like coconut husk ash (56 m^2/g), corncob ash (70 m^2/g), corn husk ash (91 m^2/g), and bamboo leaf ash (428 m^2/g), teff straw ash has a greater specific surface area. This suggests that the potential for adsorption applications of teff straw ash is higher [69, 70]. The BET surface area of the silica gels made from teff ash ranged from 592.19 to 807.16 m^2/g, which is a high value. The BET surface area rose as the teff ash's calcination temperature increased, peaking for the sample that was calcined at 700 °C. The silica gels made from teff ash have more surface area and porosity after being calcined [71]. The surface area has a significant impact on how well biosilica function. The silica gels had pore diameters ranging from 1.63 to 1.70 nm and pore volumes ranging from 0.24 to 0.34 cm^3/g. The material silica gel is robust and long-lasting, with holes that are usually 2.4 nm in size [72].

3.6.2. Fourier Transform Infra-Red Spectroscopy

Fourier Transform Infra-Red (FTIR) spectroscopy is a valuable tool for identifying the functional groups present in the material. In order to allow the ethanol to evaporate, a copper grid was covered with a preset amount of sample TSA solution and left in the dark. The TSA sample was analyzed using the FTIR spectra between 400 and 4000 cm^{-1} at ambient temperature. Figure 2 (a) displays the results of the FT-IR analysis performed on TSA samples that were heated to 500, 600, 700, 800, and 900 °C. According to the results, bending vibrations that were consistent with the current work were responsible for a band at 436 cm^{-1}, whereas Si-O-Si bond stretching was the cause of the band at 796 cm^{-1} [73]. It also implied that there was no NaCl in the solution. During the HCl washing process, all alkali, alkaline earth metals, and other contaminants were effectively eliminated.

3.6.3. X-Ray Diffraction

The broad XRD array at around 22.5° presented in Figure 2 (b), which was typical of an amorphous solid, supported the resultant silica's amorphous nature [74]. In the current study, CuK was operated between 5 and 800 at 40 kV, 44 mA, and 2θ in order to obtain XRD patterns. The XRD patterns of several ashes collected from TS are shown in Figure 4. The sample obtained at 500, 600, and 700 °C calcination temperatures had a broad peak position in this investigation that was centered about 23 °C. The current study endeavor revealed a robust broad band in which the TSA samples were discovered to be primarily amorphous. Higher peaks typically indicate higher concentrations, which are indicative of dominating phase concentrations. Based on the findings, it was determined that amorphous silica may be produced at a calcination temperature of 700 °C or lower. The observed results were supported by Palanivelu et al. [75] they looked into the paralyzed nano silica samples' tridymite and quartz crystalline states, which were shown at 800, 850, and 900 °C. These temperatures were linked to the distinctive signals observed at 20.6, 20.88, 26.5, 26.66, 27.5, 30.2, 36.1, 45.8, 50, 60, and 65°, respectively.

The XRD patterns of several silica gel samples that were manufactured at different temperatures and acquired via TSA are shown in Figure 2 (c). The extracted silica gel's amorphous nature was confirmed by the strong and broad XRD pattern discovered at 2θ = 22.5°, as shown in the figure. This quality made it ideal for use in catalysis, adsorption, and other chemical processes. The silica gel at 900 °C showed small, sharp, and powerful peaks at 2θ = 31.8°, 45.68°, and 56.72°. These peaks could have been caused by sodium chloride, which was created when the silica gel precipitated from hydrochloric acid [33]. The sol-gel process may have virtually eliminated all other constituents and transformed the crystallin silica into amorphous silica gel, as the XRD pattern has demonstrated. XRD analysis was used to verify the structural characteristics of silica gel that was made using sol-gel methods at 500, 700, and 900 °C calcination temperatures. As a result, the silica gel used in this investigation was amorphous, and the temperature range of 500–900 °C was ideal.

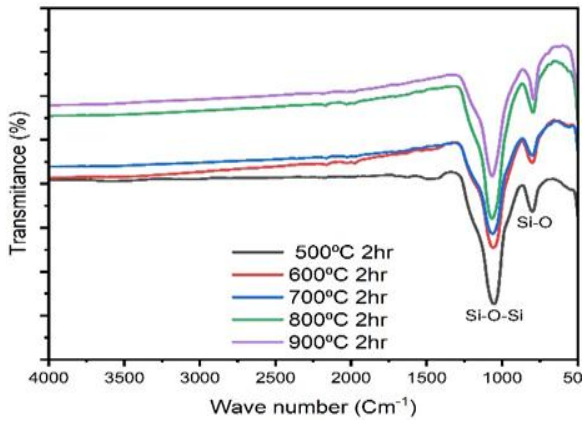

(a)

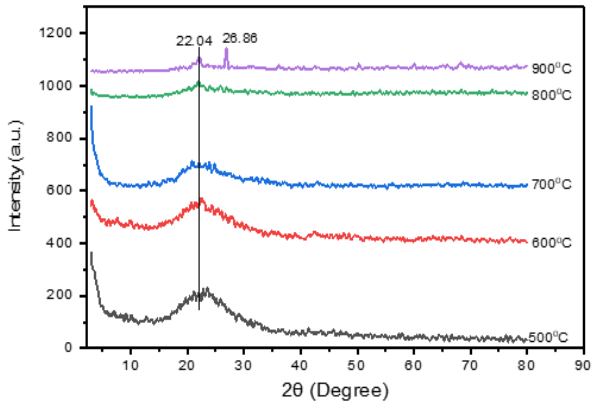

(b)

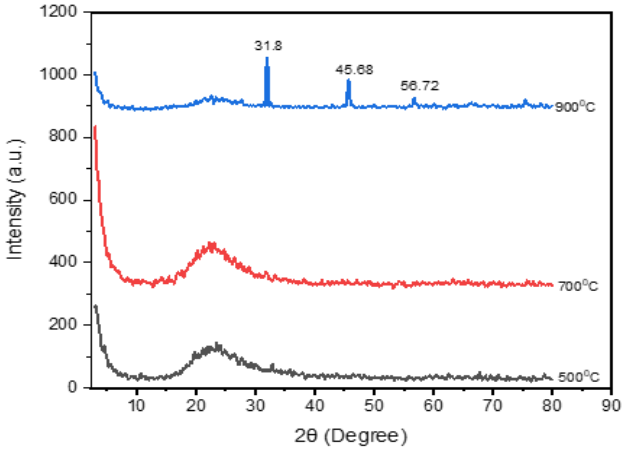

(c)

Figure 2. (a) FTIR spectra and (b) XRD patterns of TSA and (c) silica gel at different calcination temperature.

3.6.4. Scanning Electron Microscopy and Energy Dispersive X-Ray Analysis

The physical characteristics of the silica gel surface were observed using SEM images at various *2,000 magnifications. In this picture, the silica particles ranged in size of 10 µm and were arranged into clusters to produce an uneven and cohesive surface. Furthermore, larger dimensions, glossy surfaces, and a texture with dark hues were seen. Particles in alkaline-treated silica gel cluster, but particles ground in a laboratory by a deadly agent are distributed unevenly. Evidence of a small amount of incomplete combustion that left carbon impurities in the sample was shown in Figure 3) at 700 °C, shows further holes and hollow structures.

Figure 3 shows the results of an Energy Dispersive X-Ray (EDX) analysis performed on the silica gel that was manufactured from raw TS. It was discovered that oxygen, silicon, sodium, and chlorine were present in the samples. But there were evidence of the mineral's titanium and copper in the structure of the raw silica gel, or the TS. The presence of silica (SiO2) as the major constituent was confirmed by the strong intensity of Si and O deduced from the EDX spectra, as shown in Table 2. With a consistent calcination time of two hours, this indicates roughly 99.55% of the whole element. Following at 800, 500, 600, and 900 °C, respectively, are 93.84, 93.38, 85.56, and 80.25%, as shown in Table 2. There were very few other variables.

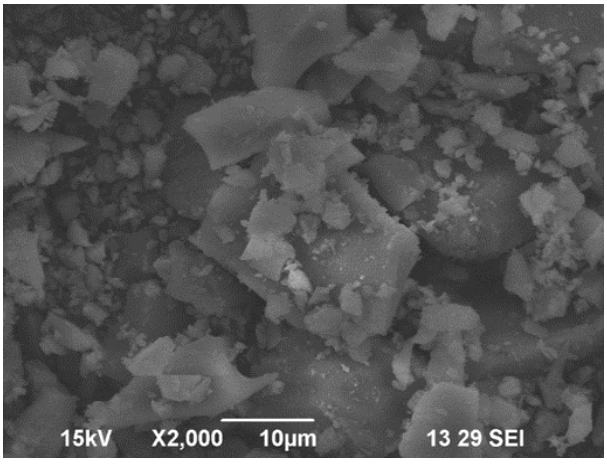

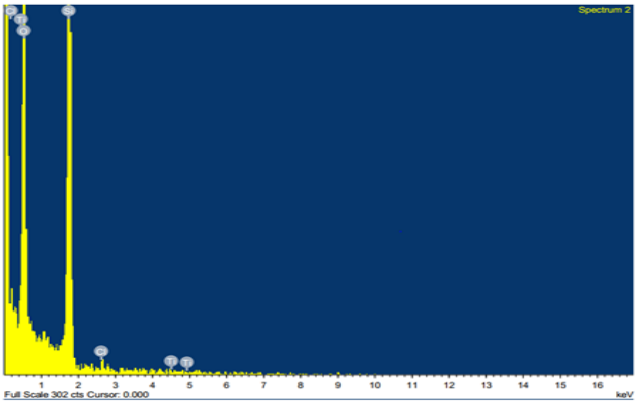

Figure 3. SEM/EDX analysis of silica gel at calcination temperature of 700 ℃ at 2 h.

Temperature (°C)	Elements (wt.%)						
	O	Si	Na	Cl	Ti	Cu	Others
500	64.54	28.84	4.26	2.25	-	-	0.11
600	59.87	25.69	8.35	6.07	-	-	0.02
700	67.42	32.13	-	0.60	-0.15	-	0.1
800	66.27	27.57	3.81	2.44	0.11	-0.21	0.1
900	56.51	23.74	12.64	7.22	-0.39	0.26	0.2

3.6.5. Characterization of modified silica gel supported silver nanoparticle

Using BET surface area analysis, the physical changes in silica following AgNPs loading and TMCS functionalization were examined. The BET surface area, pore volume, and pore diameter of the silica gel were 807.2 m^2/g, 0.34 cm^3/g, and 1.70 nm, respectively. The silica gel's surface area decreased to 510.4 m^2/g as a result of the TMCS functionalization, indicating that some of the pores in the structure were filled with TMCS radicals [76]. The surface area of the modified silica gel supported AgNPs was calculated using the BET technique. The surface area decreased as the concentration of $AgNO_3$ increased, according to the results. A, B, C, and D have surface area values of 475.0, 457.3, 438.5, and 410.9 m^2/g, in that order. This implied that some of the pores had been filled and the AgNPs had been successfully bonded to the modified silica gel surfaces.

3.6.5.1. Analysis using UV-vis spectroscopy

Both the existence of AgNPs and amino groups on the silica surface was confirmed by the absorption (a.u.) at 325 nm for the samples containing 1.5, 3, 6, and 9 mM AgNPs. The near UV absorption peak in the 240–400 nm region was likewise influenced by the amino groups [16]. Silver nanoparticles' (AgNPs') surface plasmon resonance a collective oscillation of the conduction electrons in response to incident light- determines their optical properties. AgNPs can have their size, shape, and surrounding medium changed to adjust their Surface Plasmon Resonance (SPR) band. According to earlier research, AgNPs display a distinctive surface photoluminescence peak in the visible spectrum, usually ranging from 400 to 530 nm, contingent upon the stabilizing agent and synthesis technique. AgNPs production and presence in a sample can be verified using the SPR peak as a signature. For instance, AgNPs produced with polyvinylpyrrolidone as a capping agent and sodium borohydride as a reducing agent showed an SPR peak at 452 nm in prior research. The optical properties of AgNPs are determined by their size, shape, and surface chemistry. One of the most notable features of AgNPs is the surface plasmon resonance, which is a collective oscillation of the conduction electrons in response to an incident light. This peak was attributed to the SPR phenomenon of AgNPs, which is influenced by their size, shape, and dispersion. The plant extracts improved the AgNPs' biocompatibility and eco-friendliness by acting as both stabilizing and reducing agents. Depending on the shape of the nanoparticle, the surface plasmon resonance appears as a strong absorption band in the visible portion of the spectrum, usually between 400 - 530 nm. The SPR peak at 452 nm is indicative of spherical AgNPs, as Figure 4 demonstrates. After two months, the absorbance spectra of the AgNPs-coated MSG were assessed to see how stable it was over time. Additionally, the biologically produced composites' stability was evaluated and contrasted. The findings showed that the composites held up well [3, 77].

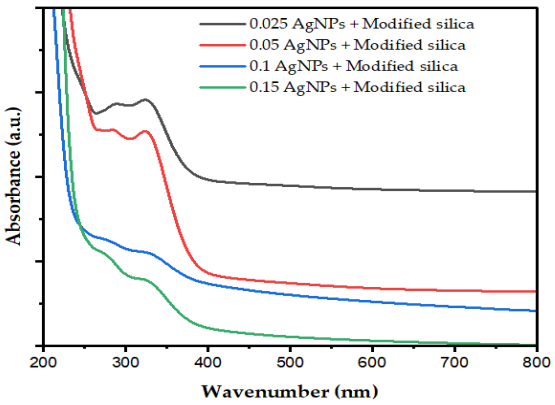

Figure 4. The UV-vis absorption spectra of biologically and sol-gel supported modified silica nanoparticles (AgNPs).

3.6.5.2. The FT-IR analysis

Two prominent peaks in the silica gel spectrum can be seen at 1,078 and 804 cm^{-1}, respectively. These represent the asymmetric and symmetric stretching vibrations of Si-O-Si. A new peak at 1,620 cm^{-1} appears in the modified silica gel spectra, suggesting the presence of $-NH_2$ groups on the surface. The AgNPs supported by modified silica gel exhibit a broad band in their spectra about 3,400 cm^{-1}. This band is thought to be caused by the O-H stretching vibrations of water molecules that have been adsorbed on the AgNPs. AgNPs' spectra have a distinct peak around 2,900 cm^{-1}, which is attributed to the capping agent's C-H stretching vibrations during the AgNPs production process. [76]. Si-O-Si bonds are visible in the modified silica gel network and are distinguished by strong and weak peaks in the 804–1077 cm^{-1} range. The C-H amplifies peak in the 1404–3134 cm^{-1} range due to the existence of Si–C bonds, which are linked to the TMCS. The absorption band linked to the H-O-H vibrations at about 1770 cm^{-1} indicates the polarity of the modified silica gel [78]. The primary bands in the AgNPs absorption spectrum were located at 3,410 and 1,640 cm^{-1}, respectively, and they corresponded to the predominant amides and -OH stretching vibrations. This suggested that phytochemical substances were stabilizing the AgNPs. Figure 5 (a) illustrates the C-H peak peaks between 1404 and 3134 cm^{-1} in the absorption spectrum of silica loaded with AgNPs. The primary amide group, the Si-O-Si stretching modes, and the carbonyl group are represented by the absorption peaks located at 1,770, 804, and 1,078 cm^{-1}, respectively. The band at 900 cm^{-1} was attributed to the Si-OH stretching mode. These spectrum characteristics show that the functionalized silica gel's amino group and AgNPs interact electrostatically, allowing AgNPs to adhere to the gel's surface via the amino group [43, 76].

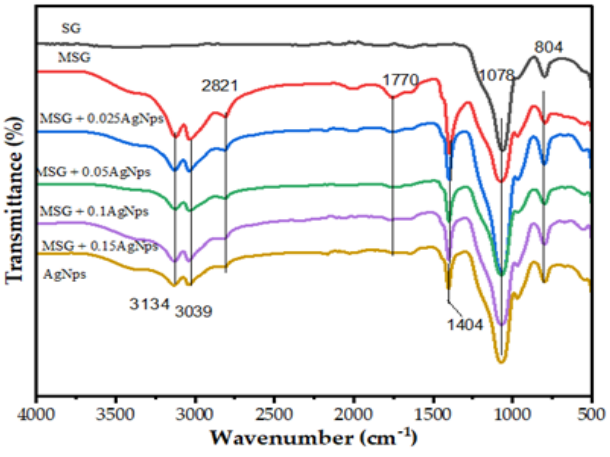

(a)

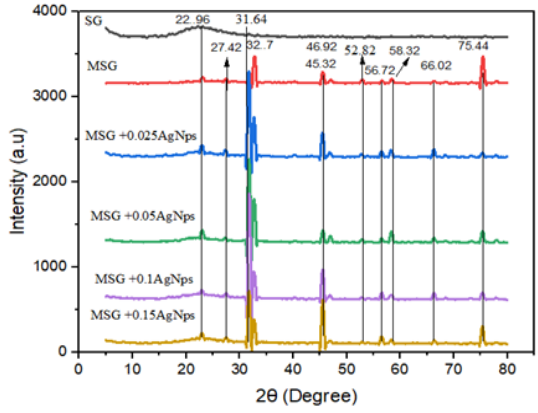

(b)

Figure 5. Results of (a) FTIR spectra and (b) XRD of SG, MSG, MSG supported at different concentration of AgNPs and AgNPs.

3.6.5.3. The XRD analysis

A strong peak at 2θ of 23° can be seen in XRD spectra presented in Figure 5 (b), suggesting that the silica gel derived from teff straw is primarily amorphous. The crystalline structure of the silica in the plant material was broken down by heating the teff straw to 700 °C for 2 h, resulting in the production of this silica gel [79].

Each crystalline phase was clearly visible in the XRD examination of the modified silica gel and the modified silica gel supported AgNPs. The modified silica gel had a well-organized structure. A significant peak was identified at 2θ values of 22.96, 27.42, 31.64, 32.7, 45.32, 46.92, 52.82, 56.72, 58.32, 66.02, and 75.44° in the XRD examination of the modified silica gel and the modified silica gel supported AgNPs generated by sol-gel technique. This suggests that the TMCS modifier, which raised the number of siloxane linkages and decreased the amount of Si-OH groups by silylation, improved the development of the structure [16, 80, 81]. In order to modify the surface, TMCS, which contains Cl- and Na+ ions, and sodium hydroxide solution are injected. The investigation showed that these ions were the cause of the peaks that formed on the modified silica gel and the modified silica gel supported AgNPs. This result implies that the shape and properties of the treated materials are significantly impacted by the surface modification method [82].

3.6.5.4. SEM/EDX analysis

The SEM images at different magnifications in Figure 6 (a) reveal the morphology of the modified silica gel surface loaded with AgNPs. The surface consists of loosely arranged honeycomb-like structures with pores of varying sizes, which is consistent with previous studies. The modification of the silica gel surface by TMCS and AgNPs treatment is evident from the SEM images of the AgNPs-impregnated modified silica gel. The SEM instrument was equipped with a component that enabled the EDX elemental analysis, which was performed after obtaining the SEM micrograph of the 9 mM Ag sample. The modified silica gel contained silver, as evidenced by a minor peak of Ag in Figure 6 (b). The deposition of the nanoparticles on the surface was supported by the presence of silver, and the EDS analysis of the SEM spectrum revealed a significant signal of silicon and oxygen corresponding to silica.

The SEM-EDS spectrum reveals the presence of various impurities in the precipitated silica gel. The impurities include Cl, Ti, Cu, and Na, which originate from different sources. The K and Al elements come from the teff straw, which is the raw material for silica extraction. The C element in carbonate form is introduced during the precipitation process, which involves adding CO_2 to the silica extract to form a carbonate compound. The POMFA also contains some C element, as well as other impurities. These elements affect the properties and quality of the precipitated silica gel [3, 83].

3.6.5.5. Antibacterial activity in batch method

This work used a batch approach to assess the antibacterial efficacy of modified silica gel containing AgNPs. In order to do this, we ran a number of tests to investigate the effects of the initial E. coli concentration, contact time, and amount of modified silica gel with AgNPs on the removal efficiency. Four different types of modified silica gel containing AgNPs (A, B, C, and D) were employed in this investigation, with one unaltered silica gel (E) serving as a control. The initial E. Col concentration was either 10^4 or $1.5*10^8$ CFU/mL, the contact time varied from 10 to 60 minutes, and the modified silica gel dosage with AgNPs was 40 mg/mL. To contrast the antibacterial properties of modified silica gel supported by AgNPs with solutions devoid of AgNPs.

When A and B were utilized for 10^4 and 10^5 CFU/mL cell suspension, the batch mode cell-killing data showed that after 30 minutes, there was no more E. coli in the treated water. For these bacterial concentrations, the modified silica gel supported AgNPs of C and D produced the same outcome after 20 and 10 minutes, respectively. When it came to A, the cell reduction was more than 99% for CFU/mL 10^7 and 10^8 and 100% for CFU/mL at 60 minutes. At 60 minutes, there was a 100% reduction for concentrations of B and C (10^6 and 10^7 CFU/mL) and a reduction of more than 98% for 10^8 CFU/mL. The findings demonstrated that, of the modified silica gel supported AgNPs of A, B, C, and D, D had the maximum antibacterial activity. D entirely. Table 3 and 4 summarizes the antibacterial performance of D against *E. coli* and *S. aureus*.

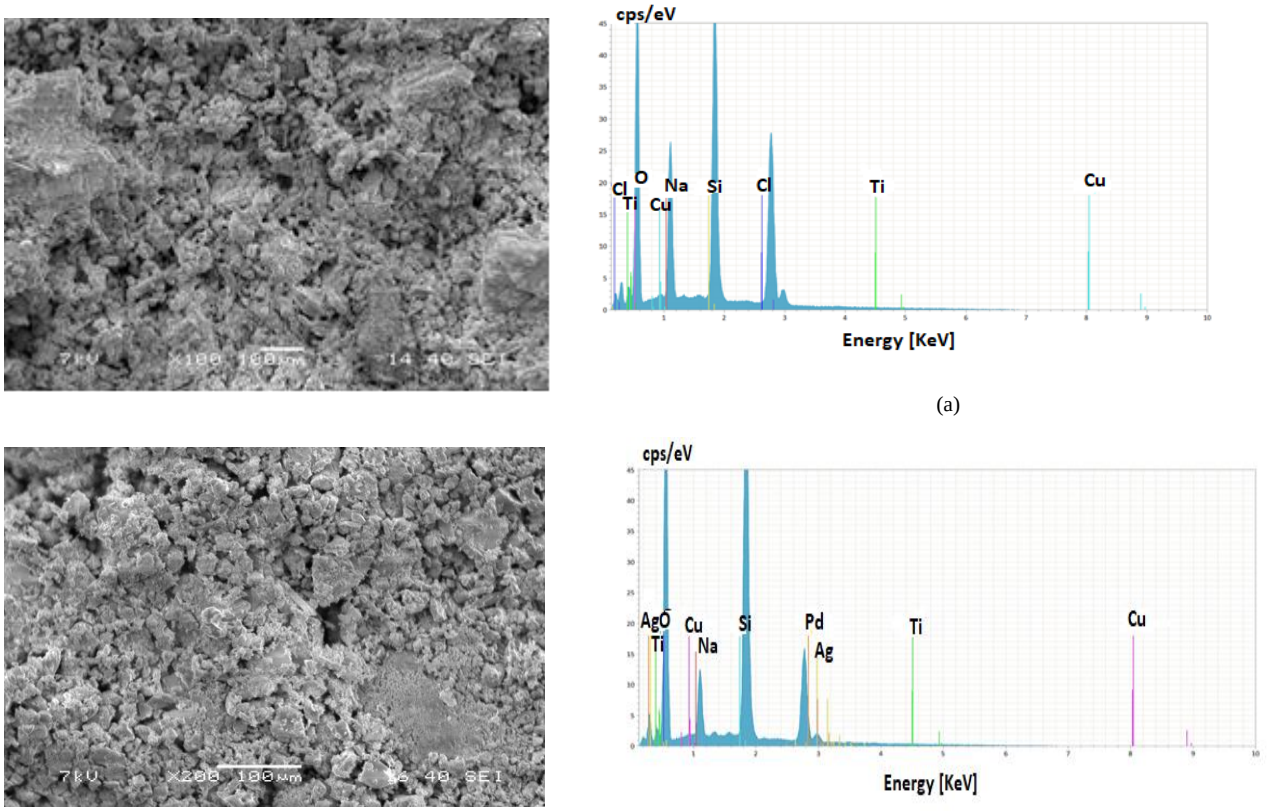

Figure 6. SEM/EDX image. (a) MSG (b) MSG supported 9 mM AgNPs.

Table 3. Test tube results for *E. coli* at different modified silica gels supported AgNPs.

E. coli CFU/mL	A (40mg/ mL)				B (40mg/mL)				C (40mg/mL)				D (40mg/mL)			
	Time (min.)				Time (min.)				Time (min.)				Time (min.)			
	10	20	30	60	10	20	30	60	10	20	30	60	10	20	30	60
10^4	1000	200	0	0	200	40	0	0	40	0	0	0	0	0	0	0
10^5	5000	400	0	0	3000	100	0	0	105	0	0	0	0	0	0	0
10^6	10^5	8000	400	0	10^5	6000	250	0	10^5	2000	200	0	800	250	100	0
10^7	10^6	10^4	2000	1	10^6	7000	340	0	10^6	3000	230	0	6000	2800	200	0
10^8	10^7	10^5	4000	9	10^7	10^4	350	3	10^7	4000	240	2	10^4	2000	150	0

Table 4. Test tube results for *E. coli* and *S. aureus* at D (30, 40 and 50 mg/mL) modified silica gels supported AgNPs.

CFU/mL	D (30mg/mL)				D (40mg/mL)				D (50mg/mL)			
	Time (min.)				Time (min.)				Time (min.)			
	10	20	30	60	10	20	30	60	10	20	30	60
E. coli												
10^5	2	0	0	0	0	0	0	0	0	0	0	0
S. aureus												
10^5	0	0	0	0	0	0	0	0	0	0	0	0

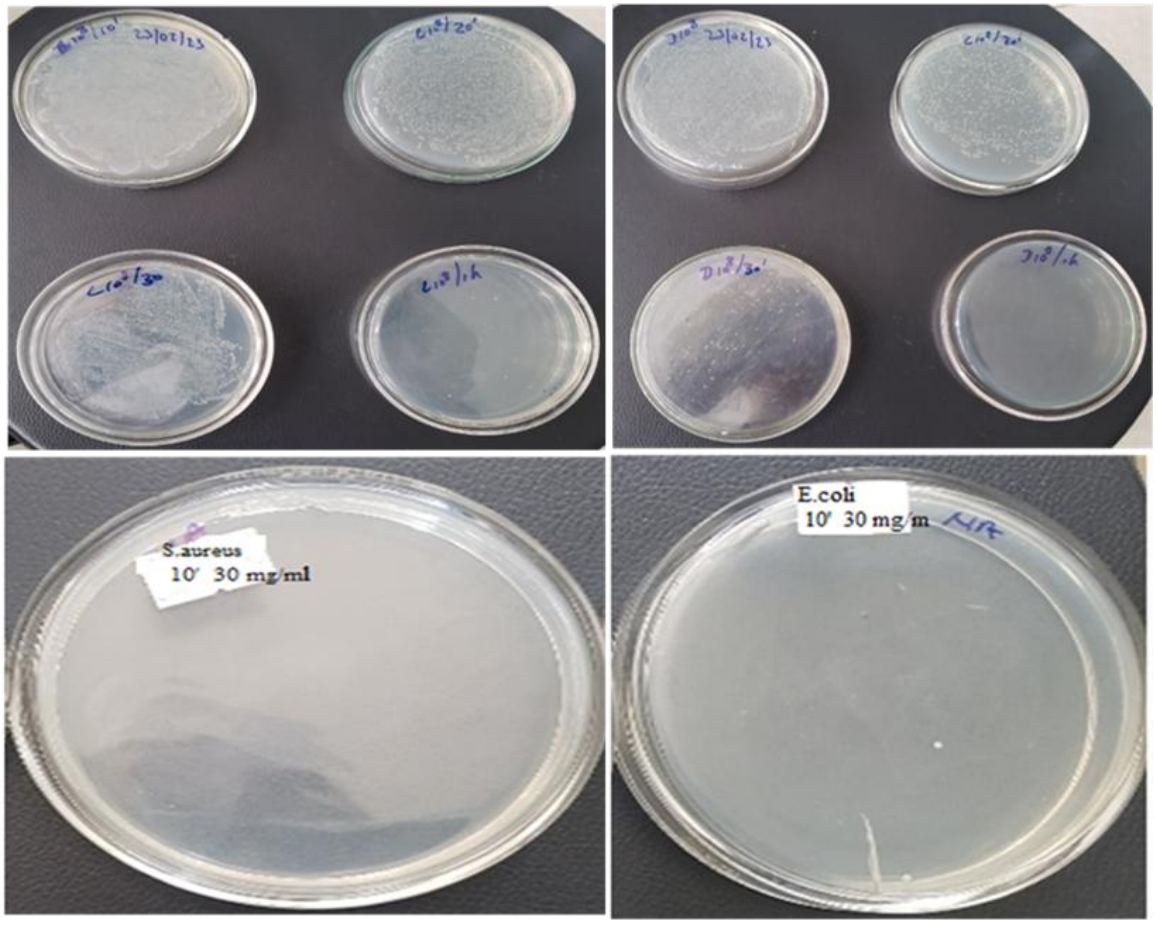

Figure 7. Test tube mode cell-killing data for (a) sample c of 10^8, (b) sample d of 10^8, (c) sample d of 10^5 *E. coli* (d) sample d of 10^5 *S. aureus*.

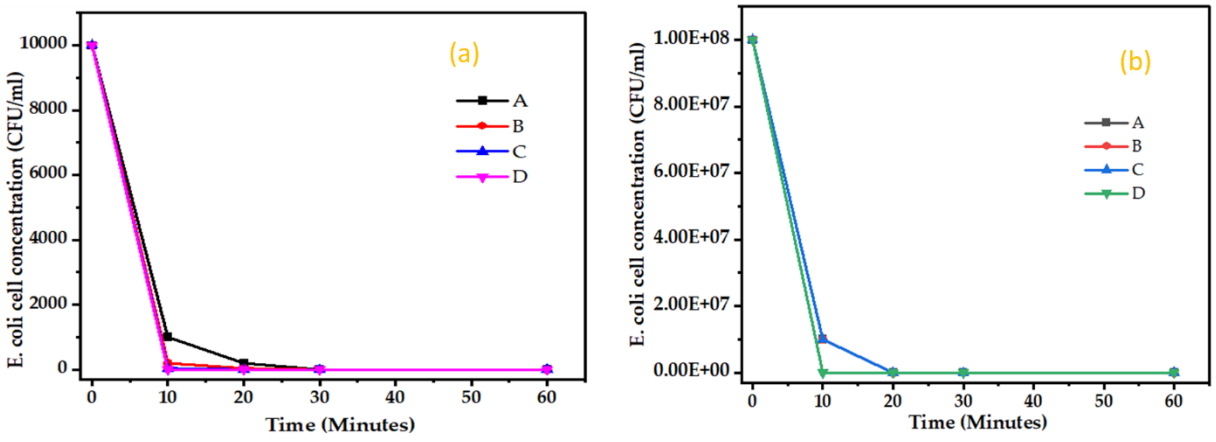

Figure 8. Test tube mode cell-killing data for (a) 10^4 and (b) 10^8 cell suspension of E. coil.

The results from the test tube experiment indicate a significant antibacterial effect of silver nanoparticles (Ag-NPBs) against E. coli bacteria. No E. coli was detected after exposure to 0.5% and 1% concentrations of Ag-NPBs for various contact times, ranging from 1 to 20 minutes based on Table 5. This contrasts sharply with the control sample of silica beads (SBs), which showed a substantial bacterial growth of approximately 4 million colony-forming units per milliliter. These findings suggest that Ag-NPBs could be a potent antibacterial agent, potentially useful in various applications where bacterial contamination is a concern. However, further research would be necessary to fully understand the implications of these results for practical applications. The data provided suggests that MSG supported AgNPs exhibit significant antibacterial activity, reducing bacterial counts from 5000 to 400 within the first 20 minutes of application. This drastic reduction to zero indicates the effectiveness of MSG-supported AgNPs in bacterial eradication, highlighting its potential as a material for water disinfection purposes. Such materials could be crucial in developing more efficient and cost-effective methods for purifying water, which is essential for health and well-being. The rapid action of the AgNPs supported by MSG suggests that this composite material could be particularly useful in scenarios where quick disinfection is required. Further research and development could optimize its application, making it a valuable tool in public health and sanitation.

Table 5. Test tube tests against bacterial suspension.

AgNPs-composite	Bacteria tested	Bacteria count after application	Retention Time (minutes)	Reference
SBA1 (0.5% Ag)	*E. coli*	0	1	[84]
		0	5	
		0	10	
		0	20	
SBA1 (1% Ag)	*E. coli*	0	1	
		0	5	
		0	10	
		0	20	
MSG (0.025 gm Ag)	*E. coli*	5000	10	Present study
		400	20	
		0	30	
		0	40	
MSG (1.5 gm Ag)	*E. coli*	0	10	
		0	20	

4. Conclusions

In the current study, modified silica gel supported silver nanoparticles (MSG-AgNPs) were synthesized for the treatment of drinking water. AgNPs was synthesized from silver nitrate ($AgNO_3$) solution and Vernonia amygdalina leaf extract for the treatment of drinking water and characterized. AgNPs were synthesized at different concentrations of $AgNO_3$ while keeping leaf extract solution constant at 10 g and characterized for its removal efficiency of removing pathogenic micro-organisms after supported by MSG. Similarly, different varieties of teff straw locally named as Filagot, Kora, Dagim, and Kuncho were used as a source of silica for the synthesis of silica gel. The varieties were treated and characterized for its silica content. Among the varieties investigated Filagot has high silica content as compared to the remaining teff straw varieties and screened for the synthesis of silica gel. Filagot teff straw was prepared, ground and a particle size under 2 μm was collected by sieving. The TS powder was further treated with HCl at different molar solutions and washed with distilled water until pH 7 and dried. Using the sol gel method, the treated powder was calcinated at different temperature of 500 to 900 ℃ at the interval of 100 ℃ for 2 h. 10 g of the calcinated TS ash was mixed with 2.5 M NaOH solution at 90 ℃ and stirred for 1 h. The solution is then treated with HCl solution in a drop wise it become neutral pH and the solution was then aged for 20 h for silica gel [52] formation. The SG with high surface area of 807.163 m^2/g achieved at 700 °C calcination was further modified to have hydrophobic properties using trimethylchlorosilane (TMCS)/ethanol/hexane at different volumetric ratio. MSG with a maximum surface area of 510.40 m^2/g was obtained at volumetric ratio of 25//25/1 of TMCS/ethanol/hexane, respectively. The modified silica gel was further used for the synthesis of MSG supported AgNPs. Then, the MSG supported AgNPs was prepared by mixing AgNPs at different concentration with MSG. 100 mL of AgNPs at different concentration was mixed with 10 g MSG for 4 h using hot plate magnetic stirrer, washed with distilled water, filtered, dried, size reduced, characterized and used as MSG supported AgNPs for the treatment of drinking water. The absorption peaks at 325 nm in the spectra were indicative of the presence of the amino group in the AgNPs-containing silica. The primary chemical groups of the silica gel were Si-O-Si, Si-OH, Si-CH, and Si-O, based on the FT-IR data. AgNPs were linked to amides and OH stretching vibrations, whereas the presence of C-H groups suggested MSG. The results of the XRD investigation showed that silica was found in all of the silica gel, MSG, and MSG-supported AgNPs. The performance of MSG-AgNPs was evaluated using batch disinfection studies against pathogenic bacteria specifically E. coli and S. aureus. For the batch study on the E. coli removal efficiency of MSG-AgNPs produced at different conditions was investigated. It was observed that MSG-AgNPs produced at 9 mM AgNPs impregnation and 40 mg of MSG-AgNPs per mL of water has demonstrated better reduction performances for different E. coli concentration at different exposure of residence time. For E. coli concentration of 104 and 105 CFU/mL and 10 min residence time as well as for E. coli concentration of 106, 107, and 108 CFU/mL, complete removal of E. coli were exhibited after 10-and 60-min residence, respectively. This study provides valuable information for various stakeholders, such as governmental organizations, non-governmental organizations, and biomedical institutes, who are concerned with preventing microbe contaminations such as E. coli and S. aureus in drinking water.

Acknowledgments

This work was financially supported by Addis Ababa Science and

Technology University, Ethiopia internal research grant (IGP 006/2023).

References

[1] Shayo, G.M., Elimbinzi, E., Shao, G.N. Fabian, C. Severity of waterborne diseases in developing countries and the effectiveness of ceramic filters for improving water quality. Bulletin of the National Research Centre, 47 (1) (2023) 113.

[2] Alegbeleye, O.O. Sant'Ana, A.S. Manure-borne pathogens as an important source of water contamination: An update on the dynamics of pathogen survival/transport as well as practical risk mitigation strategies. International journal of hygiene and environmental health, 227 (2020) 113524.

[3] Tessema, B., Gonfa, G., Hailegiorgis, S.M., Workneh, G.A. Tadesse, T.G. Synthesis and evaluation of the anti-bacterial effect of modified silica gel supported silver nanoparticles on E. coli and S. aureus. Results in Chemistry, 7 (2024) 101471.

[4] Tessema, B., Gonfa, G. Hailegiorgis, S.M. Synthesis of Modified Silica Gel Supported Silver Nanoparticles for the Application of Drinking Water Disinfection: A Review. Results in Engineering, (2024) 102261.

[5] El-Aassar, A.H., Said, M., Abdel-Gawad, A. Shawky, H. Using silver nanoparticles coated on activated carbon granules in columns for microbiological pollutants water disinfection in Abu Rawash area, Great Cairo, Egypt. Australian journal of basic and applied sciences, 7 (1) (2013) 422-32.

[6] Phong, N.T.P., Thanh, N.V.K. Phuong, P.H., editors. Fabrication of antibacterial water filter by coating silver nanoparticles on flexible polyurethane foams. Journal of Physics: Conference Series; 2009: IOP Publishing.

[7] Ali, Z.H. Al-Fatlawi, A.H. Efficiency of silver nano particles in removing Escherichia coli ATCC 25922 from drinking water distribution pipes. Results in Engineering, 17 (2023) 100988.

[8] Salim, A., Shetty, K.S., Febin, H., Sameed, N., Pal, S., Nair, B.G. Madhavan, A. Lytics broadcasting system: A novel approach to disseminate bacteriophages for disinfection and biogenic hydrogen sulphide removal tested in synthetic sewage. Results in Engineering, 13 (2022) 100314.

[9] Ojha, A. Nanomaterials for removal of waterborne pathogens: Opportunities and challenges. Waterborne pathogens, (2020) 385-432.

[10] Neme, I., Gonfa, G. Masi, C. Castor seeds hull activated carbon impregnated with silver nanoparticles for removal of Escherichia coli from water. Case Studies in Chemical and Environmental Engineering, 7 (2023) 100320.

[11] González-Castaño, M., De Miguel, J.N., Sinha, F., Wabo, S.G., Klepel, O. Arellano-Garcia, H. Cu supported Fe-SiO2 nanocomposites for reverse water gas shift reaction. Journal of CO2 Utilization, 46 (2021) 101493.

[12] Mahesh, B. A comprehensive review on current trends in greener and sustainable synthesis of ferrite nanoparticles and their promising applications. Results in Engineering, (2023) 101702.

[13] Zhang, X.-F., Liu, Z.-G., Shen, W. Gurunathan, S. Silver nanoparticles: synthesis, characterization, properties, applications, and therapeutic approaches. International journal of molecular sciences, 17 (9) (2016) 1534.

[14] Payami, R., Ghorbanpour, M. Parchehbaf Jadid, A. Antibacterial silver-doped bioactive silica gel production using molten salt method. Journal of Nanostructure in Chemistry, 6 (3) (2016) 215-21.

[15] Tessema, B., Gonfa, G., Hailegiorgis, S.M., Prabhu, S.V. Manivannan, S. Synthesis and characterization of silver nanoparticles using reducing agents of bitter leaf (Vernonia amygdalina) extract and tri-sodium citrate. Nano-Structures & Nano-Objects, 35 (2023) 100983.

[16] Thamilselvi, V. Radha, K.V. Silver nanoparticle loaded silica adsorbent for wastewater treatment. Korean Journal of Chemical Engineering, 34 (6) (2017) 1801-12.

[17] Bruna, T., Maldonado-Bravo, F., Jara, P. Caro, N. Silver nanoparticles and their antibacterial applications. International Journal of Molecular Sciences, 22 (13) (2021) 7202.

[18] Quang, D.V., Sarawade, P.B., Jeon, S.J., Kim, S.H., Kim, J.-K., Chai, Y.G. Kim, H.T. Effective water disinfection using silver nanoparticle containing silica beads. Applied Surface Science, 266 (2013) 280-7.

[19] Nwajuaku, I.I. Agunwamba, J.C. Evaluating the aeration efficiency of hydraulic flume on photo-oxidative disinfection of wastewater. Results in Engineering, 20 (2023) 101455.

[20] Sarker, M.Z., Rahman, M.M., Minami, H., Suzuki, T., Hossain, M.K. Ahmad, H. Mesoporous amine functionalized SiO2 supported Cu nanocatalyst and a kinetic-mechanistic degradation study of azo dyes.Colloids and Surfaces A: Physicochemical and Engineering Aspects, 617 (2021) 126403.

[21] Ghadimi, M., Zangenehtabar, S. Homaeigohar, S. An overview of the water remediation potential of nanomaterials and their ecotoxicological impacts. Water, 12 (4) (2020) 1150.

[22] Abou - El - Sherbini, K.S., Amer, M.H., Abdel - Aziz, M.S., Hamzawy, E.M., Sharmoukh, W. Elnagar, M.M. Encapsulation of biosynthesized nanosilver in silica composites for sustainable antimicrobial functionality. Global Challenges, 2 (10) (2018) 1800048.

[23] Tesfaye Gari, M., Tessema Asfaw, B., Arumugasamy, S.K., Deso Abo, L. Jayakumar, M. Natural resources-based activated carbon synthesis. Encyclopedia of Green Materials: Springer; 2023. p. 1-11.

[24] Li, W.-L., Fu, P., Lin, W.-T., Zhang, Z.-L., Luo, X.-W., Yu, Y.-H., Xu, Z.-K. Wan, L.-S. High-performance thin-film composite (TFC) membranes with 2D nanomaterial interlayers: An overview. Results in Engineering, (2024) 101932.

[25] Parandhaman, T., Das, A., Ramalingam, B., Samanta, D., Sastry, T., Mandal, A.B. Das, S.K. Antimicrobial behavior of biosynthesized silica–silver nanocomposite for water disinfection: A mechanistic perspective. Journal of hazardous materials, 290 (2015) 117-26.

[26] Asfaw, B.T., Gari, M.T., Jeyapaul, A.S., Jayakumar, M. Baskar, G. Volarization of agro farm yard waste into bioenergy: present state and future directions. Biofuels and Bioenergy: Elsevier; 2025. p. 173-201.

[27] Raanan, R., Zack, O., Ruben, M., Perluk, I. Moshe, S. Occupational Silica Exposure and Dose–Response for Related Disorders—Silicosis, Pulmonary TB, AIDs and Renal Diseases: Results of a 15-Year Israeli Surveillance. International Journal of Environmental Research and Public Health, 19 (22) (2022) 15010.

[28] Murugadoss, S., Lison, D., Godderis, L., Van Den Brule, S., Mast, J., Brassinne, F., Sebaihi, N. Hoet, P.H. Toxicology of silica nanoparticles: an update. Archives of toxicology, 91 (9) (2017) 2967-3010.

[29] Tesserae, B., Gonfa, G., Mekuria Hailegiorgis, S. Venkatesa Prabhu, S. An Overview of Current and Prognostic Trends on Synthesis, Characterization, and Applications of Biobased Silica.Advances in Materials Science and Engineering, 2023 (2023) 4865273.

[30] Gari, M.T., Asfaw, B.T., Abo, L.D., Jayakumar, M. Kefalew, G. Effective Utilization of Agricultural Cereal Grains in Value-Added Products: A Global Perspective. Value Added Products from Food Waste: Springer; 2024. p. 41-58.

[31] Tessema, A.B., Tesfaye, G.M., Ayenew, A., Fikade, T. Hailemichael, S. Optimizing the removal of chromium from aqueous solution by adsorption using sugarcane bagasse. Research Journal of Water Pollution & Purification Research, 6 (2) (2019) 22-36.

[32] Morales-Paredes, C.A., Rodríguez-Linzán, I., Saquete, M.D., Luque, R., Osman, S.M., Boluda-Botella, N. Manuel, R.-D.J. Silica-derived materials from agro-industrial waste biomass: Characterization and comparative studies. Environmental Research, 231 (2023) 116002.

[33] Bageru, A.B. Srivastava, V.C. Biosilica preparation from abundantly available African biomass Teff (Eragrostis tef) straw ash by sol-gel method and its characterization. Biomass Conversion and Biorefinery, 8 (4) (2018) 971-8.

[34] Asfaw, B.T., Gari, M.T., Jayakumar, M. Baskar, G. Sustainable Bioethanol Production from the Pretreated Waste Lignocellulosic Feedstocks. Circular Bioeconomy Perspectives in Sustainable Bioenergy Production: Springer; 2024. p. 377-94.

[35] Tessema, B., Gonfa, G., Hailegiorgis, S.M. Prabhu, S.V. Characteristic investigations on bio-silica gel prepared from teff (eragrostis tef) straw: effect of calcination time. Materials Research Express, 10 (11) (2023) 115102.

[36] Shewatatek, S., Gonfa, G., Mekuria, S. Tessema, B. Response Surface Optimization of Lead Adsorption onto Teff Straw-Derived Activated Carbon. Results in Surfaces and Interfaces, (2024) 100378.

[37] International, A., ASTM D3173/D3173M-17a Standard Test Method for Moisture in the Analysis Sample of Coal and Coke: ASTM International West Conshohocken, PA, USA; [2017].

[38] Designation, A. D 3175 Standard Test Method for Volatile Matter in the Analysis Sample of Coal and Coke. Annual Book of Standards. PA: ASTM. USA, (2017)

[39] ASTM, ASTM D-3174-93-Standard test method for ash in the analysis sample of coal and coke from coal: Annual Book of ASTM Standards; [1988].

[40] Kalapathy, U., Proctor, A. Shultz, J. A simple method for production of pure silica from rice hull ash. Bioresource Technology, 73 (2000) 257-62.

[41] Tessema, B., Gonfa, G., Hailegiorgis, S.M. Prabhu, S.V. Synthesis and characterization of biosilica gel produced from teff (Eragrostis tef) straw using the sol-gel technique. Bioresource Technology Reports, (2023) 101497.

[42] Norsuraya, S., Fazlena, H. Norhasyimi, R. Sugarcane bagasse as a renewable source of silica to synthesize santa barbara amorphous-15 (SBA-15). Procedia engineering, 148 (2016) 839-46.

[43] Abdul Halim, Z.A., Mat Yajid, M.A. Hamdan, H., editors. Synthesis and characterization of rice husk ash derived-silica aerogel beads prepared by ambient pressure drying. Key Engineering Materials; 2016: Trans Tech Publ.

[44] Tessema, B., Gonfa, G., Hailegiorgis, S.M. Prabhu, S.V. Synthesis and Characterization of Modified Silica Gel from Teff Straw Ash Using Sol-gel Method. Next Materials, (2024) 100146.

[45] Basem, A., Jasim, D.J., Majdi, H.S., Mohammed, R.M., Ahmed, M. Al-Rubaye, A.H. Adsorption of Heavy Metals from Wastewater by Chitosan: A Review. Results in Engineering, (2024) 102404.

[46] Mohamad, N.F., Rani, N.H.A., Elham, O.S.J., Muhamad, S.H.A., Muda, S.A., Basear, Y. Faisal, M.K.M., editors. Synthesis and characterization of silica aerogel from rice husk with ambient pressure drying method. Journal of Physics: Conference Series; 2020: IOP Publishing.

[47] Khojasteh-Taheri, R., Ghasemi, A., Meshkat, Z., Sabouri, Z., Mohtashami, M. Darroudi, M. Green Synthesis of Silver Nanoparticles Using Salvadora persica and Caccinia macranthera Extracts: Cytotoxicity Analysis and Antimicrobial Activity Against Antibiotic-Resistant Bacteria. Applied Biochemistry and Biotechnology, (2023) 1-16.

[48] Wang, L., He, H., Zhang, C., Sun, L., Liu, S. Yue, R. Excellent antimicrobial properties of silver-loaded mesoporous silica SBA-15. Journal of applied microbiology, 116 (5) (2014) 1106-18.

[49] Shin, Y.-S., Park, M., Kim, H.-Y., Jin, F.-L. Park, S.-J. Synthesis of silver-doped silica-complex nanoparticles for antibacterial materials. Bulletin of the Korean Chemical Society, 35 (10) (2014) 2979-84.

[50] Tessema, B., Gonfa, G., Hailegiorgis, S.M. Sundramurthy, V.P. Characterization of teff straw from selected teff varieties from Ethiopia. Heliyon, 9 (6) (2023)

[51] Wassie, A.B. Srivastava, V.C., editors. Synthesis and characterization of nano-silica from teff straw. Journal of Nano Research; 2017: Trans Tech Publ.

[52] Amibo, T.A., Beyan, S.M. Damite, T.M. Production and optimization of bio-based silica nanoparticle from teff straw (eragrostis tef) using rsm-based modeling, characterization aspects, and adsorption efficacy of methyl orange dye.Journal of Chemistry, 2022 (2022)

[53] Setiawan, W.K. Chiang, K.-Y. Crop residues as potential sustainable precursors for developing silica materials: a review. Waste and Biomass Valorization, 12 (5) (2021) 2207-36.

[54] Wassie, A. Srivastava, V.C. Chemical treatment of teff straw by sodium hydroxide, phosphoric acid and zinc chloride: adsorptive removal of chromium. International journal of environmental science and technology, 13 (2016) 2415-26.

[55] Assefa, E.G., Kiflie, Z. Demsash, H.D. Valorization of Abundantly Available Ethiopian Teff (Eragrostis Tef) Straw for the Isolation of Cellulose Fibrils by Alkaline Hydrogen Peroxide Treatment Method. Journal of Polymers and the Environment, (2022) 1-13.

[56] Bagherzade, G., Tavakoli, M.M. Namaei, M.H. Green synthesis of silver nanoparticles using aqueous extract of saffron (Crocus sativus L.) wastages and its antibacterial activity against six bacteria. Asian Pacific Journal of Tropical Biomedicine, 7 (3) (2017) 227-33.

[57] Bhardwaj, A., Hossain, S. Majhi, M.R. Preparation and characterization of clay bonded high strength silica refractory by utilizing agriculture waste. boletín de la sociedad española de cerámica y vidrio, 56 (6) (2017) 256-62.

[58] Anuar, M.F., Fen, Y.W., Zaid, M.H.M., Matori, K.A. Khaidir, R.E.M. Synthesis and structural properties of coconut husk as potential silica source. Results in Physics, 11 (2018) 1-4.

[59] Azizi, S.N., Dehnavi, A.R. Joorabdoozha, A. Synthesis and characterization of LTA nanozeolite using barley husk silica: Mercury removal from standard and real solutions. Materials Research Bulletin, 48 (5) (2013) 1753-9.

[60] Umeda, J. Kondoh, K. High-purification of amorphous silica originated from rice husks by combination of polysaccharide hydrolysis and metallic impurities removal. Industrial crops and products, 32 (3) (2010) 539-44.
[61] Çepelioğullar, Ö. Pütün, A.E. A pyrolysis study for the thermal and kinetic characteristics of an agricultural waste with two different plastic wastes. Waste management & research, 32 (10) (2014) 971-9.
[62] Adebisi, J.A., Agunsoye, J.O., Bello, S.A., Kolawole, F.O., Ramakokovhu, M.M., Daramola, M.O. Hassan, S.B. Extraction of silica from sugarcane bagasse, cassava periderm and maize stalk: Proximate analysis and physico-chemical properties of wastes. Waste and Biomass Valorization, 10 (3) (2019) 617-29.
[63] Trninić, M., Jovović, A. Stojiljković, D. A steady state model of agricultural waste pyrolysis: A mini review. Waste Management & Research, 34 (9) (2016) 851-65.
[64] Bageru, A.B. Srivastava, V. Preparation and characterization of biosilica from teff (eragrostis tef) straw by thermal method. Materials Letters, 206 (2017) 13-7.
[65] Ishmah, S.N., Permana, M.D., Firdaus, M.L. Eddy, D.R. Extraction of silica from bengkulu beach sand using alkali fusion method. PENDIPA Journal of Science Education, 4 (2) (2020) 1-5.
[66] Ding, Y. Su, D. Purifying native in-situ mastoid SiO2 from rice husk. Energy procedia, 16 (2012) 1269-74.
[67] Faizul, C., Abdullah, C. Fazlul, B. Extraction of silica from palm ashvia citric acid leaching treatment. Advances in Environmental Biology, 7 (12) (2013) 3690-5.
[68] Hossain, S.S., Mathur, L. Roy, P. Rice husk/rice husk ash as an alternative source of silica in ceramics: A review. Journal of Asian Ceramic Societies, 6 (4) (2018) 299-313.
[69] Rangaraj, S. Venkatachalam, R. A lucrative chemical processing of bamboo leaf biomass to synthesize biocompatible amorphous silica nanoparticles of biomedical importance. Applied Nanoscience, 7 (5) (2017) 145-53.
[70] Prempeh, C.O., Formann, S., Schliermann, T., Dizaji, H.B. Nelles, M. Extraction and Characterization of Biogenic Silica Obtained from Selected Agro-Waste in Africa. Applied Sciences, 11 (21) (2021) 10363.
[71] Elanthikkal, S., Mohamed, H.H. Alomair, N.A. Extraction of biosilica from date palm biomass ash and its application in photocatalysis. Arabian Journal of Chemistry, 16 (3) (2023) 104522.
[72] Hamza, T.A., Sherif, A.H. Abdalla, E.A. A novel approach to reinforce provisional material using silica gel powder. Stomatological Disease and Science, 1 (2017) 3-7.
[73] Mor, S., Manchanda, C.K., Kansal, S.K. Ravindra, K. Nanosilica extraction from processed agricultural residue using green technology. Journal of Cleaner Production, 143 (2017) 1284-90.
[74] Imoisili, P.E., Ukoba, K.O. Jen, T.-C. Green technology extraction and characterisation of silica nanoparticles from palm kernel shell ash via sol–gel. Journal of Materials Research and Technology, 9 (1) (2020) 307-13.
[75] Palanivelu, R., Padmanaban, P., Sutha, S. Rajendran, V. Inexpensive approach for production of high-surface-area silica nanoparticles from rice hulls biomass. IET nanobiotechnology, 8 (4) (2014) 290-4.
[76] Themselves, V. Radha, K.V. Silver nanoparticle loaded silica adsorbent for wastewater treatment.Korean Journal of Chemical Engineering, 34 (2017) 1801-12.
[77] Tessema, B., Gonfa, G. Mekuria, S. Preparation of modified silica gel supported silver nanoparticles and its evaluation using zone of inhibition for water disinfection. Arabian Journal of Chemistry, (2024) 106036.
[78] Abdul Halim, Z.A., Mat Yajid, M.A., Idris, M.H. Hamdan, H. Effects of silica aerogel particle sizes on the thermal–mechanical properties of silica aerogel–unsaturated polyester composites. Plastics, Rubber and Composites, 46 (4) (2017) 184-92.
[79] Gu, S., Zhou, J., Yu, C., Luo, Z., Wang, Q. Shi, Z. A novel two-staged thermal synthesis method of generating nanosilica from rice husk via pre-pyrolysis combined with calcination. Industrial Crops and Products, 65 (2015) 1-6.
[80] Chiarakorn, S., Areerob, T. Grisdanurak, N. Influence of functional silanes on hydrophobicity of MCM-41 synthesized from rice husk. Science and Technology of Advanced Materials, 8 (1-2) (2007) 110.
[81] Nyabadza, A., Mc Donough, L.M., Manikandan, A., Ray, A.B., Plouze, A., Muilwijk, C., Freeland, B., Vazquez, M. Brabazon, D. Mechanical and antibacterial properties of FDM additively manufactured PLA parts. Results in Engineering, 21 (2024) 101744.
[82] Wu, X., Fan, M., Mclaughlin, J.F., Shen, X. Tan, G. A novel low-cost method of silica aerogel fabrication using fly ash and trona ore with ambient pressure drying technique. Powder Technology, 323 (2018) 310-22.
[83] Utama, P.S., Yamsaengsung, R. Sangwichien, C. Production and characterization of precipitated silica from palm oil mill fly ash using CO_2 impregnation and mechanical fragmentation. Brazilian Journal of Chemical Engineering, 36 (2019) 523-30.
[84] Quang, D.V., Sarawade, P.B., Hilonga, A., Kim, J.-K., Chai, Y.G., Kim, S.H., Ryu, J.-Y. Kim, H.T. Preparation of silver nanoparticle containing silica micro beads and investigation of their antibacterial activity. Applied Surface Science, 257 (15) (2011) 6963-70.